King's Research Portal

Exploiting the Morphology of a Shape Memory Spring as the *Active Backbone* of a Highly Dexterous *Tendril Robot* (*ATBR*)

Kayode Sonaike* and S.M.Hadi Sadati*, Christos Bergeles, Ian D. Walker

Abstract— Tendrils are common stable structures in nature and are used for sensing, actuation, and geometrical stiffness modulation. In this paper, for the first time we exploit the helical geometry of a shape memory alloy (SMA) tendril as a simple to fabricate highly dexterous robotic continuum tentacle that we called Active Tendril-Backbone Robot (ATBR). This is achieved via partial (120 deg) activation of single helix turns resulting in backbone directional bendings. A 141.5 mm prototype (130 mm when fully compressed) has been fabricated and a simple theoretical framework is proposed and experimentally validated for modeling of the tentacle configuration. The manipulator has five 2-DOF joints capable of reaching bending angles of up to 54.5 deg and angular speed of up to 6.8 deg/s. The dexterity of the manipulator is showcased empirically in reaching complex configurations and simple navigation through confined space of a curving path.

Keywords- Tendril, Continuum manipulator, Dexterous robot, Shape Memory Alloy, Morphological contribution.

Fig. 1: Complex shapes resulted from actuating (local heating) different joints along an ATBR.

I. INTRODUCTION

Performing complicated tasks such as manipulation in unpredictable conditions where safe interaction with the environment is important requires dexterity and compliance. In such tasks, low actuation energy, high dexterity, reachability, maneuverability, back drivability and self-adjustability of continuum mechanisms are shown to be advantageous. Continuum manipulators are novel robotic archetypes, presenting a single continuous backbone structure with a compliant backbone. Interest in these single form robotic manipulators began as early as the 1960's [1], in which Anderson and Horn's Tensor arm was developed for underwater exploration. Since then, numerous contributions towards continuum manipulator research have been made, facilitated by the development of soft actuators. The actuation mechanism of this class of manipulators has been always at the center of scientific debate. Some of the recent designs are inflatable tendon driven backbones [2], braided extensile pneumatic actuators [3], braided hydraulic actuators [4], braided pneumatic actuators in a silicon body shell [5], shrinkable design with antagonistic tendon and pneumatic actuation [6], long tendon driven tendril [7], bioinspired SMA actuators [8], and origami structure backbones [9]. The tendon driven and pneumatically or hydraulically actuated designs suffer from routing complexities, bulky external power supply and control units, and limitations in designing highly dexterous

systems. Smart materials, artificial muscles, and shape memory structures on the other hand are usually hard to fabricate.

Recently, a new field of research, so-called "embodied intelligence", "morphological contribution" or "morphological computation", has emerged wherein the physical body morphology is exploited to simplify the perception and control tasks [10]. In this context, the tendril is one of the most studied structures in biology and zoology [11] for their interesting morphological properties such as geometrical compliance. Bioinspired tendril morphologies are utilized as robot backbone [7], actuator [8], stiffness controllable interfaces [12], [13], [14], and fiber optics based bending sensors [15], [16] for continuum robots. SMA tendrils (sometimes known as artificial muscles) are used as single actuation units[8], [17].

In this paper, for the first time, we utilize the partial actuation of a single SMA tendril to achieve multiple local directional bending (Fig. 1). The SMA helix is considered both as the manipulator backbone and actuator and named Active Tendril-Backbone Robot (ATBR). Despite the aforementioned means of actuation, an ATBR actuation principle and fabrication are simple, affordable, and compact. The actuation process is as simple as connecting a flexible electric wires to the activation site (120 deg portion of a single helix turn covered with heat shrink) and one to the tendril base. The SMA shape change is achieved through local heating of the covered area by the heat shrink, that we suspect is due to high current local sparks at the wire connection points, while the rest of the tendril remains intact due to insufficient Joule heating effect (increasing temperature of
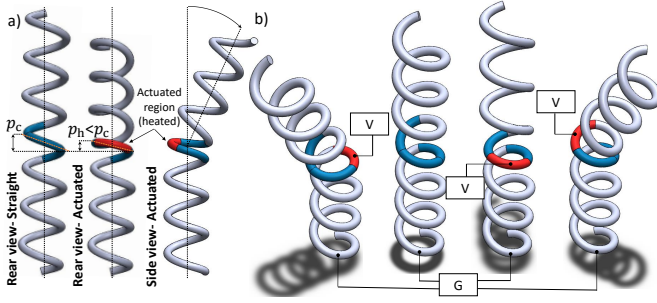
Fig. 2: Working principle of a single full turn of a SMA tendril as an independent 3-DOF joint. The SMA tendril is compressed when heated. a) Rear and side view of the tendril when one third (120 deg) of a full turn is activated (heated- in red). A twist along this section results a reduction in the helix pitch on the opposite side and hence bending the backbone in the opposite direction. b) Wiring diagram for different activation scenarios. V- power supply connection through a relay board and PWM current controller, G-permanent ground connection red- active (heated) section, blue-inactive (cold) section.

a metal through passing electrical current). As a result, the backbone bends due to local change of the tendril pitch. Each single turn of the tendril can be turned into an independent 3-DOF joint (two side bendings and axial shrinkage) along the continuum arm forming a highly dexterous continuum arm. As the proof of concept, a continuum arm is fabricated with five sets of triple-wires along the tendril. A simple theoretical framework based on identification of the SMA tendril properties and Constant Curvature (CC) assumption is proposed for modeling of the manipulator.

In the rest of this paper, first the the manipulator working principle and design are discussed in section II. A simple modeling framework is discussed in section III. Experimental study and simulation validations are presented in section IV followed by a short discussion on our future plans. Finally conclusions are presented in section VI.

II. MANIPULATOR WORKING PRINCIPLE & DESIGN

A one-way SMA tendril was used as both the backbone structure and actuator for the continuum manipulator. The tendril had 0.9 mm wire diameter, 5.4 mm coil mean diameter and 80 mm length when fully collapsed. The tendril was extended to 141.5 mm, in which the tendril pitch ($p = l/n$-tendril length l to number of turns n ratio) is 6.741 mm and coil mean diameter was reduced to 4.69 mm, and undergone shrinkage when heated. Fig. 2 shows the ATBR working principle and actuation wiring diagram. The experimental setup, control diagram, and modeling framework are presented in Fig. 3.

A. Local Directional Bending

A uniform change in a tendril pitch results in a uniform elongation or contraction. On the other hand, local partial (e.g. one-third of a full turn) modulations through local heating results in lateral bending of the backbone toward the opposite direction of the activated section (Fig. 2-a). Having three equally spaced activation regions of 120 deg (by connecting three actuation wires), each full turn acts as

a local independent 3-DOF joint (Fig. 2-b). The number of joints can be as many as the number of turns in the tendril.

B. Local Heating

Control wires (three per joint) were passed through the center of the helix, turned around the SMA tendril wire at the connection point, and covered with two layers of heat shrink to stay in place. A single wire at the tendril base was connected to the ground pin of the electrical current control module. Connecting any of the control wires to the power supply resulted in electrical current between the wire connection point all the way to the tendril base. We observed that by fixing the supply current to 1 A, the electrical power was not enough to heat the entire SMA tendril through Joule heating. However, this current was enough to observe local heating in the area around the active wire connection point that is covered by a heat shrink (see the supplementary media files). Since the same area around the other inactive wire connection points was not heated, we suspect that the current was high enough to form micro-sparks at the connection site. As a result, local heat is generated and accumulated, due to heat insulation by the heat shrink cover, causing a local change in the wire temperature and consequently SMA wire deformation. This way, for the first time, we programmed a SMA morphology by design to locally response (in the form of generating local heat) to a dispersed electrical signal that propagates throughout the material. The exact mechanism behind the observed local heating is subject to further investigation in the future. Five single-turn bending sections, each with three control wires, were created along the SMA tendril. A total of 16 wires were used.

C. SMA Tendril Selection

To simplify the controller mechatronic design, the chosen SMA tendril retained its configurations after the activation. As a result, the control wires could be activated one at a time with a single electrical current control unit that was connected to the wires through a set of timed relay switches. This limited the manipulator load bearing capacity to an amount that does not deform the inactive SMA tendril. Hence this control architecture is better for tasks involving known limited external load.

Furthermore, the material shape memory response to heat should be faster than its thermal conductivity. A low response and highly thermal conductive SMA results in uniform distribution of heat, and hence deformation, even when it is locally heated. The load bearing requirement of the inactive SMA tendril, and the material shape memory response vs. thermal conductivity limit the available choices for a useful tendril. Through testing different tendril sizes and material, we could find a suitable one-way SMA tendril with a fully collapsed state as its programmed (heated) shape. As a side effect of such choice, an activated section was collapsed and could not retain its initially elongated configuration. This problem can be addressed by introducing a secondary SMA tendril with elongated programmed shape to elongate back the tendril after it is collapsed. Alternatively, a compression
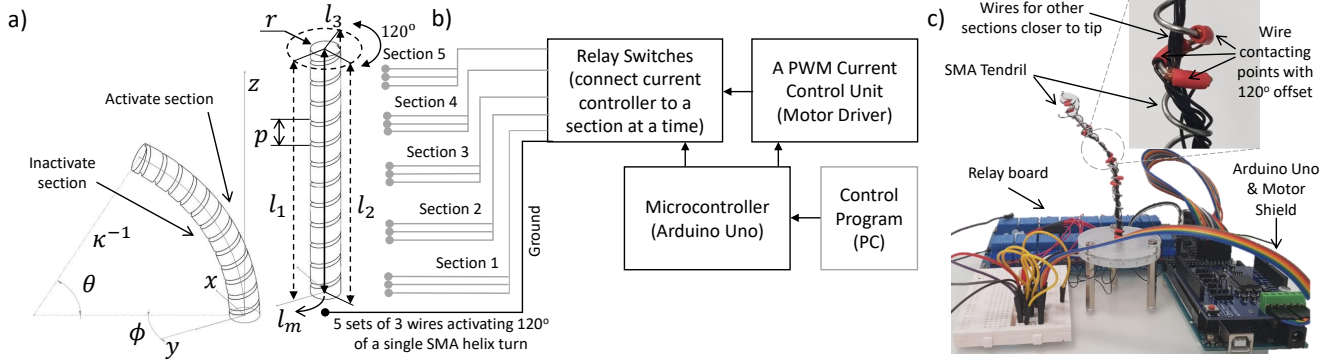
Fig. 3: ATBR diagrams, (a) Constant Curvature modeling framework, (b) a simple feed-forward control structure that actuate one wire at a time, (c) experimental setup design.

$$T_j(\kappa, l, \phi) = \begin{bmatrix} \cos(\kappa l)\cos(\phi)^2 + \sin(\phi)^2 & \cos(\kappa l)\cos(\phi)\sin(\phi) - \cos(\phi)\sin(\phi) & \sin(\kappa l)\cos(\phi) & -(\cos(\phi)(\cos(\kappa l) - 1))/\kappa \\ \cos(\kappa l)\cos(\phi)\sin(\phi) - \cos(\phi)\sin(\phi) & \cos(\phi)^2 + \cos(\kappa l)\sin(\phi)^2 & \sin(\kappa l)\sin(\phi) & -(\sin(\phi)(\cos(\kappa l) - 1))/\kappa \\ -\sin(\kappa l)\cos(\phi) & -\sin(\kappa l)\sin(\phi) & \cos(\kappa l) & \sin(\kappa l)/\kappa \\ 0 & 0 & 0 & 1 \end{bmatrix} \tag{1}$$

elastic backbone can be introduced to force a pitch increase (elongation) in the bent opposing side of the helix when a section is bent. Activation of this elongated portion results in the bent to become straight again. We will address these issues and design considerations in more details in a future design.

D. Controller Design

A simple control setup was implemented based on an Arduino Uno micro-controller and an L298P Arduino Motor Shield to control the supply current. The current control unit was connected to control wires (denoted by V in Fig. 2-b) through a 40 V 16-channel relay board one at a time. Pulsed Width Modulated (PWM) signals were used to supply fixed 1 A electric current (supploed through a current power supply) to each control wire. Compared to a constant voltage power supply, providing fixed current resulted in unified energy transfer to the material regardless of the SMA wire length. The relay board was used in a normally-open configuration and controlled in an on/off fashion for a controlled amount of time (10 s for identification tests and 5 s for reaching complex configurations) using the Arduino Uno micro-controller board. A control program was developed using Arduino IDE which commands the relay and motor driver shield through the IDE standard serial protocol. A complex desired shape was achieved through sequential activation of the sections in the right amount of time found based on identification of the SMA tendril thermal properties. This simple control structure was possible since the SMA backbone holds its shape in place after every activation sequence.

III. KINEMATIC MODELING & SIMULATION STUDY

There exist a variety of modeling approaches for the mechanics of continuum manipulator in the literature, such as lumped system methods, Constant and Variable Curvature assumptions, reduced-order methods [18], [19]. Among them, the Constant Curvature (CC) assumption is probably the more broadly applicable method allowing for closed-form computation of the manipulator forward and inverse kinematics [20]. This approach approximates the backbone
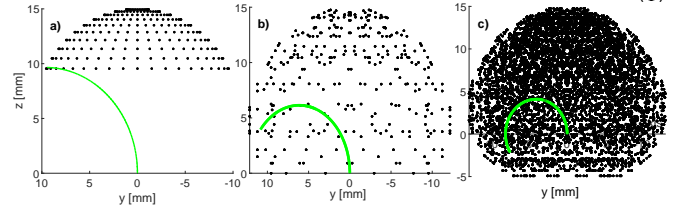

Fig. 4: Work-space (black dots) difference between a manipulator with one, two, and three independent sections for similar overall length, maximum curvature, and change in the curve parameters.

as a constant curvature curve with curvature κ_j, length l_j and bending plane angle ϕ_j as the curve parameters. The manipulator kinematic transformation consists of a transformation from the actuator space to the configuration (curve) space (robot specific mapping), followed by a transformation from the configuration space to Cartesian (task) space (robot independent mapping). Fig. 3-a presents the CC parameters used in this study.

The robot independent mapping is presented by a transformation matrix $T_m = T_j.T_l$ for each individual section, where T_j is a joint (single helix turn) CC kinematics as in Eq. 1 [20], T_l is the linear transformation associated with an inactive straight section of length $l_l = n_l p$, n_l is the number of inactive turns in a section. See Table I for the experimental setup parameters.

The robot specific mapping consists of two steps, a mapping from local variation of the tendril pitch Δp to the length of three imaginary actuation lines $l_{j_i}, i \in [1, 3]$ (Fig. 3.a), and a mapping from l_j to the CC parameters. Each imaginary line lies on a circle with coil mean radius ($r = 2.325$ mm) on the opposite side of a set of 120 deg sections. The former is easily identifiable from the thermal identification of the tendril as

$$l_{j_i} = l_{j_0} - n_j \Delta p_i, \tag{2}$$

where $n_j = 1/3$ is the number of active turns (here one-third of a full turn is active at a time), $l_{j_0} = n_j p$ is the joint initial length, and Δp_i is the change in the pitch of the ith 120 deg segment of the joint. An empirical relation for $\Delta p - t$ will
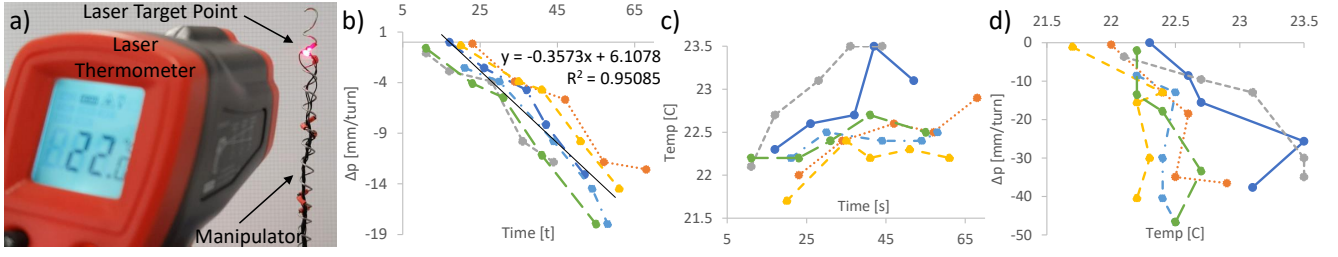
Fig. 5: Thermal properties identification of the SMA tendril, (a) a laser thermometer pointing at the active coils, (b) change in the pitch vs. time $\Delta p - t$, (c) temperature vs. time $T - t$, (d) and pitch vs. temperature $\Delta p - T$ for different experimental trials (different colors) with a single tendril turn.
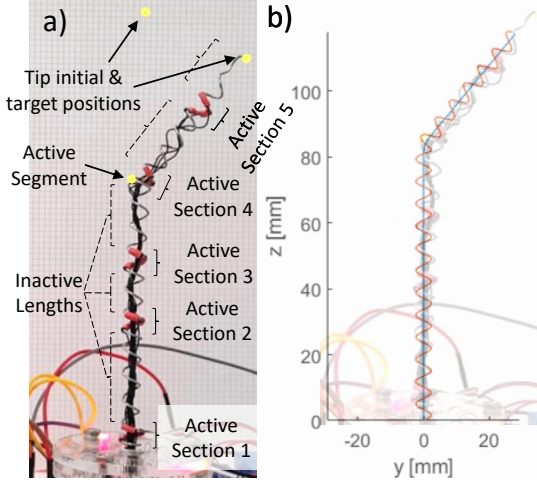

Fig. 6: (a) Single section bending experiment of the manipulator versus (b) simulation results (actuation time: 10 s).

be identified. The latter mapping is as in [20]

$$
\begin{aligned}
l_j &= \sum_{i=1}^{3} l_{j_i}, \ \phi_j = \operatorname{atan}\left(\frac{\sqrt{3}(l_{j_2} + l_{j_3} - 2l_{j_1})}{3(l_{j_2} - l_{j_3})}\right), \quad (3) \\
\kappa_j &= \frac{2\sqrt{l_{j_1}^2 + l_{j_2}^2 + l_{j_3}^2 - l_{j_1}l_{j_2} - l_{j_1}l_{j_3} - l_{j_2}l_{j_3}}}{r(l_{j_1} + l_{j_2} + l_{j_3})}.
\end{aligned}
$$

Fig. 4 shows the comparison of three tendril manipulators with same length but one, two, and three independent active sections but similar overall length, maximum curvature, and change in the curve parameters. The plots show significant improvements in the work-space volume and manipulator manipulability (denser reachable space) as the manipulator dexterity increases.

The presented modeling framework is the simplest possible for an ATBR. A more detailed model for constant curvature bending of a tendril is presented in our previous work [21].

IV. EXPERIMENTAL IDENTIFICATION & VALIDATIONS

A. SMA Thermal Properties Identification

The tendril pitch variation δp and actuation velocity versus time t and local temperature $\mathcal{T}$ were experimentally identified through analyzing video recordings of the tendril in controlled uniform activation of a full turn of the SMA tendril. A 30 fps camera, set up to minimize the parallax error, was used to capture a recording of the backbone during actuation which is latter analyzed using openCV.

A non-contact laser thermometer, as the easiest way to measuring the surface temperature, was placed at a distance close enough to capture the temperature reading and tendril deformation within the same camera video frame (Fig. 5.a). The helix pitch angle was determined based on the backbone displacement measurement.

Fig. 5.b-d shows the identification experiment setup and result plots for $\Delta p - t$, $T - t$, and $\Delta p - \mathcal{T}$ relations in six different trials with similar conditions. The inefficiency of our temperature measurements technique has resulted in scattered plots for $\mathcal{T} - t$ and $\Delta p - \mathcal{T}$, while the $\Delta p - t$ plot shows an almost linear relation identified as

$$
\begin{aligned}
\Delta p &= (-0.3573C_1)t + (6.1078 + C_2) \quad (4) \\
&= (-0.3573C_1)(t - t_0 - C_3),
\end{aligned}
$$

in mm/turn with mean $R^2 = 0.9508$, where $t_0 = 17.1$ s is the system thermal lag, and C_i are individual correction coefficients for each joint.

Observing the unreliable measured temperature dependent relations, we substitute Eq. 2 in Eq. 2 for model and control the change in the local pitch based on the section activation time. This is more suited to our simple feed-forward control architecture where there is no need for a temperature sensor. We left more accurate identification of the temperature relations for a further study.

B. Individual Joints' Correction Coefficients

Fig. 6 shows experiments on simple activation of second segment of the 4th joint for 10 s. Individual correction coefficients C_i are found for each Joins' segment by comparing the experimental and simulation results as in Fig. 6.b. The identified values are presented in Table I. The manipulator is capable of reaching a bending angles of up to 54.5 deg (mean 34 deg) with a angular speed of up to 6.8 deg/s (mean 4.3 deg/s) disregarding the thermal lag (t_0 & C_3).

C. Complex Configurations' Experiments & Simulations

Six random combinations of the actuation of the manipulator different joints were tested (approximate values are listed in Table I) to showcase the dexterity of the proposed design and to validate our modeling framework. The simulation results proved accurate in predicting the overall deformation concodering teh correction coefficients (Fig. 7). More detailed analysis of the modeling and control errors is left for a future work. Hysteresis in the material,
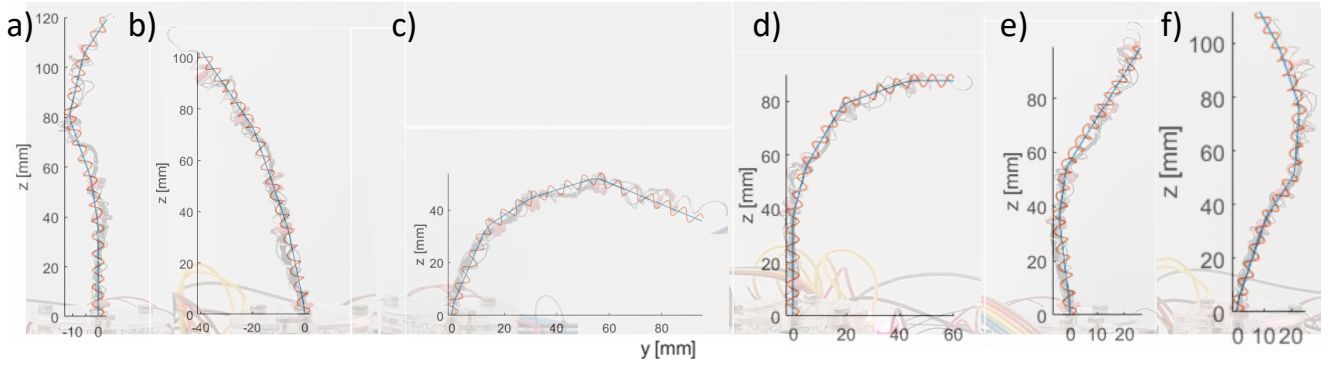
Fig. 7: Complex deformations of the ATBR according to the approximate input values in Table I, in comparison with the numerical simulations.

V. DISCUSSION & FUTURE WORK

variation in the initial configuration of the tendril when manually extended after each experiment, and variation in the environment factors such as room temperature and humidity are the possible causes of such errors.

As a proof-of-concept design, we have demonstrated the capabilities of a novel highly dexterous miniature continuum manipulator by exploiting the helical geometry of a SMA tendril as the manipulator backbone and actuators. Possible applications of this design include inspection of confined spaces in environments with limited variation in temperature and proper natural cooling, e.g. underwater inspection, inspection in cold places such as poles, mountain tops, caves, and Space. For such applications, usually a small camera would be attached at the tip of the manipulator as a fixed tip load to be considered in the SMA tendril selection process. Alternatively, such a manipulator, with its easy and cheap to build design and control architecture, can be a good subject for studying continuum manipulators kinematics, control, and design. Fig. 8 shows a sample implementation of navigating in an imaginary narrow port. We plan to conduct more practical experiments in our future study.

A. Design Limitations

Currently, the presented ATBR needs to extended back manually to an initial fully extended configuration after each round of activation. This problem can be tackled by introducing a compression elastic beam as the manipulator backbone that preserves an initially elongated shape for the tendril when no section is activated. In this case, the SMA tendril should be strong enough to bend the elastic core when activated but soft enough to follow its shape when inactive. Alternatively, two way shape memory tendrils with suitable thermal and mechanical elasticity properties can be used.

Such designs requires constant activation of the joints to keep a deformed configuration. A simpler solution could be using two concentric SMA tendrils but with opposing programmed shapes. Such tendrils should be fully compliant to the opposing tendril movement when inactive but stiff enough to move the opposing tendril when active. Thermal insulation between the tendrils and extra wires to control both of them should be considered.

TABLE I: Setup parameters and approximate activation time for six random control input combinations as in Fig. 7. The 1st module is the closes to the base.

Sec.	n_l	Seg.	C_1	C_3	a	b	c	d	e	f
			Trial Label→		Approx. Activation Time [s]					
1	4	1	0.465	-15.1	0	0	25	0	0	20
		2	0.795	-15.1	0	15	0	0	10	0
		3	1.252	-16.1	0	0	0	0	0	0
2	2	1	1.697	-16.1	0	0	10	5	5	5
		2	1.68	-14.1	0	5	0	0	0	0
		3	2.008	-16.1	5	0	0	0	0	0
3	3	1	2.027	-15.1	0	0	5	5	10	0
		2	2.383	-14.1	5	0	0	0	10	10
		3	1.201	-14.1	0	0	0	0	0	10
4	3	1	2.254	-15.1	5	0	10	10	0	0
		2	2.357	-15.1	0	0	0	0	0	0
		3	2.89	-15.1	0	5	0	0	0	10
5	2	1	2.868	-14.1	5	0	0	5	0	0
		2	2.504	-14.1	0	0	0	0	0	5
		3	3.095	-15.1	0	0	0	0	0	0

We rely on natural air convection in room temperature for our tests. A proper cooling mechanism is needed to achieve fast enough reactivation cycles depending on the application, e.g. this may not be a problem for underwater or application in very cold places.

The same control architecture as in Section II-D can be used if two opposing tendrils are used as explained above. However, the use of a passive inner backbone or a double-way SMA tendril would require maintaining a joint temperature constant for maintaining any configuration. This requires a closed-loop temperature controller relying on implementation of temperature sensors which is an issue due to space limitations, wiring complexity, and commercially available sensor sizes. Such control structure requires more than one current control unit or very fast switching of the relay board to maintain the sections temperature in a very slow PWM fashion.

B. Future Work

In further research, we will address the limitations with the design and control architecture. On the design front, we will investigate the possible usage of two opposing one-way SMA tendrils. A more thorough theoretical study based on differential geometry of the tendril and the variable curvature kinematics of the backbone will assist with investigating the effect of payload on the proposed manipulator. The SMA behavior is subject to hysteresis properties of the material and the environmental changes in temperature and humidity. A detailed model of the material properties and behavior
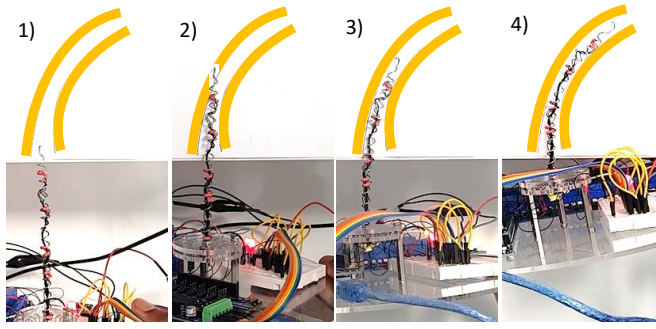
Fig. 8: Sequences of a sample navigation task in an imaginary confined pathway. The pathways imaginary walls are drawn on a paper to prevent any interaction with the manipulator that may result in passive deformation of the backbone. The manipulator base moves upward while the backbone sections are activated sequentially to comply with the curved pathway.

will assist taking these effect into consideration or suggesting an automated tuning mechanism in the form of an adaptive control architecture. Detailed error analyses are required regarding different aspects of this research, e.g. validation of the theoretical framework, payload bearing capability of the device, motion repeatability, accuracy of the control architecture, temperature estimation, etc. The addition of these features would allow for increased functionality of the proposed manipulator.

VI. Conclusion

We have presented a proof-of-concept design for a novel, easy to build and affordable continuum manipulator named Active Tendril-Backbone Robot (ATBR). We utilized the morphology of a SMA helix tendril, as both the manipulator backbone and actuator, and local heating in response to general dispersed electrical current throughout the material via structural design. Each full turn of the helical backbone can act as a 3-DOF joint by local activation of one-third of the full turn. Our miniature manipulator is 4.69 mm in diameter, elongated to 141.5 mm length, lightweight, and features five bending sections capable of reaching approximate bending angles of up to 54.5 deg and angular speeds of up to 6.8 deg/s. A simple modeling framework based on the Constant Curvature assumption is proposed and successfully verified through simulations and experimental study. The presented manipulator is unique in design with minimal fabrication efforts, yet demonstrates noteworthy potential for inspection tasks in environments with proper natural cooling and for educational purposes.

References

[1] I. D. Walker, "Continuous Backbone "Continuum" Robot Manipulators," *International Scholarly Research Notices (ISRN Robotics)*, vol. 2013, p. e726506, July 2013.

[2] W. McMahan, et al., "Design and implementation of a multi-section continuum robot: Air-octor," in *2005 IEEE/RSJ International Conference on Intelligent Robots and Systems, IROS*, pp. 3345–3352, 2005.

[3] W. McMahan, et al., "Field trials and testing of the OcotArm continuum manipulator," in *Proceedings of the 2006 IEEE international conference on robotics and automation (ICRA)*, pp. 2336–2341, 2006.

[4] I. S. Godage, et al., "Novel modal approach for kinematics of multisection continuum arms," in *IEEE International Conference on Intelligent Robots and Systems (IROS)*, (San Francisco, California, USA), pp. 1093–1098, IEEE, 2011. 00034.

[5] M. Cianchetti, et al., "Soft Robotics Technologies to Address Shortcomings in Today's Minimally Invasive Surgery: The STIFF-FLOP Approach," *Soft Robotics*, vol. 1, no. 2, pp. 122–131, 2014.

[6] F. Maghooa, et al., "Tendon and pressure actuation for a bio-inspired manipulator based on an antagonistic principle," in *2015 IEEE International Conference on Robotics and Automation (ICRA)*, (Seattle, WA, USA), pp. 2556–2561, IEEE, May 2015.

[7] J. S. Mehling, et al., "A minimally invasive tendril robot for in-space inspection," in *Proceedings of the First IEEE/RAS-EMBS International Conference on Biomedical Robotics and Biomechatronics, 2006, BioRob 2006*, vol. 2006, (Pisa, Italy), pp. 690–695, IEEE, 2006. 00035.

[8] C. Laschi, et al., "Soft Robot Arm Inspired by the Octopus," *Advanced Robotics*, vol. 26, no. 7, pp. 709–727, 2012.

[9] S.-J. Kim, et al., "An origami-inspired, self-locking robotic arm that can be folded flat," *Science Robotics*, vol. 3, p. eaar2915, Mar. 2018.

[10] R. M. Füchslin, et al., "Morphological Computation and Morphological Control: Steps Toward a Formal Theory and Applications," *Artificial Life*, vol. 19, pp. 9–34, Nov. 2012.

[11] S. J. Gerbode, et al., "How the Cucumber Tendril Coils and Overwinds," *Science*, vol. 337, pp. 1087–1091, Aug. 2012.

[12] Y.-J. J. Kim, et al., "A novel layer jamming mechanism with tunable stiffness capability for minimally invasive surgery," *IEEE Transactions on Robotics*, vol. 29, pp. 1031–1042, Aug. 2013.

[13] S. Sadati, et al., "Stiffness Control of Soft Robotic Manipulator for Minimally Invasive Surgery (MIS) Using Scale Jamming," in *Intelligent Robotics and Applications*, Lecture Notes in Computer Science, pp. 141–151, Springer, Cham, Aug. 2015.

[14] S. Sadati, et al., "Three-Dimensional-Printable Thermoactive Helical Interface With Decentralized Morphological Stiffness Control for Continuum Manipulators," *IEEE Robotics and Automation Letters*, vol. 3, pp. 2283–2290, July 2018.

[15] S. Sareh, et al., "Bio-inspired tactile sensor sleeve for surgical soft manipulators," in *2014 IEEE International Conference on Robotics and Automation (ICRA)*, pp. 1454–1459, May 2014.

[16] R. Xu, et al., "Curvature, Torsion, and Force Sensing in Continuum Robots Using Helically Wrapped FBG Sensors," *IEEE Robotics and Automation Letters*, vol. 1, pp. 1052–1059, July 2016.

[17] Y. Kim, et al., "Active Stiffness Tuning of a Spring-Based Continuum Robot for MRI-Guided Neurosurgery," *IEEE Transactions on Robotics*, vol. 34, pp. 18–28, Feb. 2018.

[18] S. Sadati, et al., "Mechanics of Continuum Manipulators, a Comparative Study of Five Methods with Experiments," in *Towards Autonomous Robotic Systems*, vol. 10454, (Surrey, UK), pp. 686–702, Springer International Publishing, 2017.

[19] S. H. Sadati, et al., "TMTDyn: A Matlab package for modeling and control of hybrid rigid–continuum robots based on discretized lumped systems and reduced-order models," *The International Journal of Robotics Research*, p. 0278364919881685, Jan. 2020.

[20] R. J. Webster and B. A. Jones, "Design and Kinematic Modeling of Constant Curvature Continuum Robots: A Review," *The International Journal of Robotics Research*, vol. 29, no. 13, pp. 1661–1683, 2010.

[21] S. Sadati, et al., "A Geometry Deformation Model for Braided Continuum Manipulators," *Front. Robot. AI*, vol. 4, 2017.